Supplementary Information *for*

Factors Affecting Iodine Emission from the Reactive Uptake of Ozone to Simulated Seawater

Stephanie R. Schneider[1], Pascale S. J. Lakey[2], Manabu Shiraiwa[2], Jonathan P. D. Abbatt[1,]*

[1]Department of Chemistry, University of Toronto, 80 St. George Street Toronto, ON, Canada.

[2]Department of Chemistry, University of California, Irvine, California 92697, United States

Table of Contents

Experimental set-up

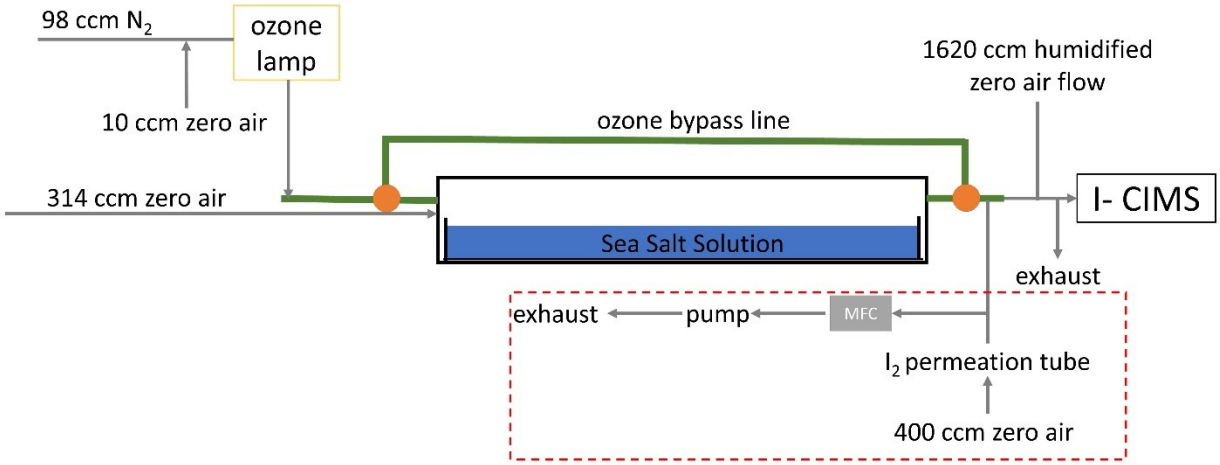

Figure S1: Experimental configuration. The orange circles represent the three-way valves used to switch the flow of ozone between the flow tube containing the salt solution and the bypass line. The calibration set up is highlighted by the red dashed box. MFC = mass flow controller, ccm = cubic centimeters per minute.

I-CIMS Calibration

The I-CIMS was calibrated by introducing a variable amount of $I_{2(g)}$ from a perm tube containing $I_{2(s)}$ to the system. The additional set-up for the calibration is presented in the red box in Figure S1. The flows in the red box were in addition to the other experimental flows, which meant that ozone was present during the calibration to create conditions identical to experimental conditions. It also helped us calibrate for any losses in the tubing downstream of the flow tube, and the instrument. The I_3^- ion signal was normalized to the sum of the signals of the iodide (I^-) ion and the iodide-water cluster ($I{\bullet}H_2O^-$).

In the presence of ozone, gas phase iodide (the reagent ion) can react to form iodine oxides (IO^-). This has been previously reported in the literature.[1,2] IO^- can cluster with analytes to be detected as an analyte•IO^- cluster. At our experimental ozone mixing ratios of ~100 ppb, the IO^- and I_3^- signal are well correlated as shown in Figure S2.B. We also see the charge transfer product of I_2^- that is well correlated to I_3^- signal as well, as shown in Figure S2.A. Importantly, the I_3^- signal is

linearly correlated with mixing ratio of $I_{2(g)}$ at constant ozone concentrations, as shown in Figure S3. For these experiments, we only used the I_3^- signal to quantify $I_{2(g)}$, however it is important to note the specific chemistry that is occurring to prevent the misidentification of other peaks.

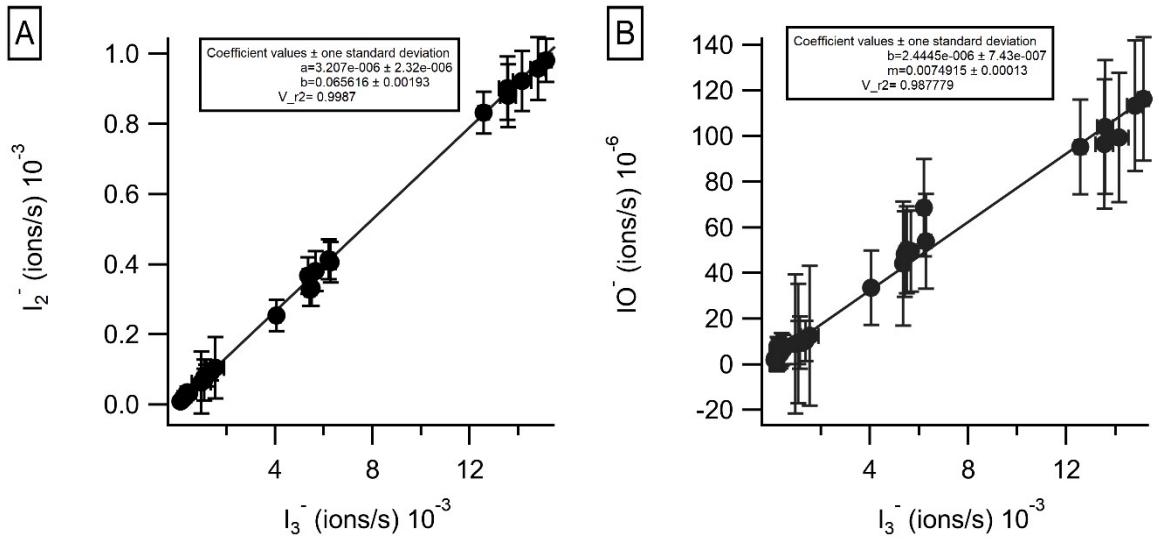

Figure S2: Panel A shows the relationship between the I_2^- and I_3^- signal during the calibration of the I-CIMS. Panel B shows the relationship between the IO^- and I_3^- signal during the calibration.

Before each experiment, the I-CIMS was calibrated quickly with a two-point calibration (0.1 ppb and 1 ppb in the instrument) to ensure a similar sensitivity to the more robust calibration, an example of which is in Figure S3.

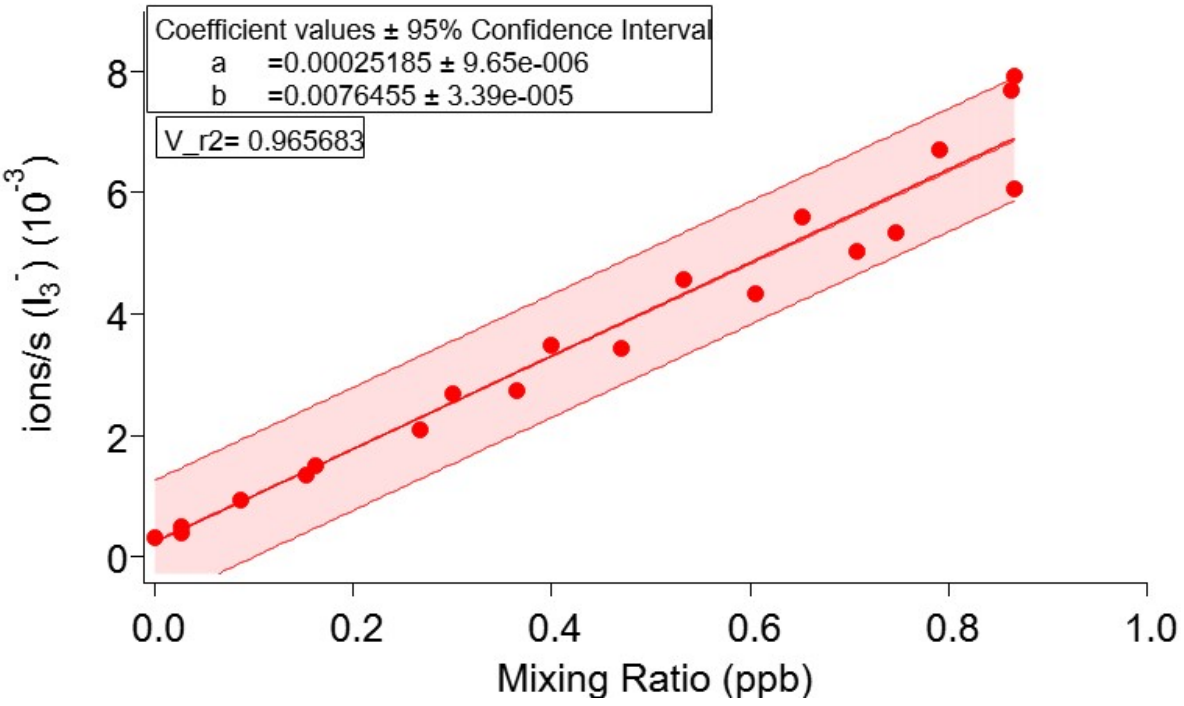

Figure S3: Linear calibration of the measured I_3^- ion normalized to the iodide and the iodide water cluster ions as a function of the mixing ratio of $I_{2(g)}$. The limit of detection (LOD) was calculated by taking 3 times the standard deviation of zero air through the experimental set-up, which averaged 2.2 ± 0.5 ppt for the instrument.

TEP and Carbohydrate Measurements

The surface microlayer of our culture was sampled using the glass slide method, as described previously.[3] Measurements of the total carbohydrates were made according to the methods of Myklestad et al.[4] Briefly, the cultures were heated in an alkaline environment, before addition of Fe^{3+}. Fe^{3+} is reduced by the monosaccharides into Fe^{2+}. Afterwards, 2,4,6-tripyridyl-s-triazine (TPTZ) is added to complex with the Fe^{2+} which is measured spectrophotometrically. To measure the polysaccharides, the glycosidic bonds were hydrolysed, and the difference before and after hydrolysis represents the contribution of the polysaccharides. A measurement comparing the transparent exopolymer (TEP) measurements in the bulk and surface microlayer of *Thalassiosira pseudonana* was made previously.[5]

In the ocean, there are a wide range of concentrations of both TEP and carbohydrates. For carbohydrates, some studies using the same method have measured values in the Norwegian

ocean between 4-10 µmol C L^{-1}, which well above what we measure in the *Thalassiosira pseudonana* cultures.[4] Measurements of TEP in ocean samples using our methods range from 200 – 8000 µg Xantham Gum equivalents L^{-1},[6] which is again orders of magnitude below our measurements between 40,000 – 200,000 µg Xeq L^{-1}.[5]

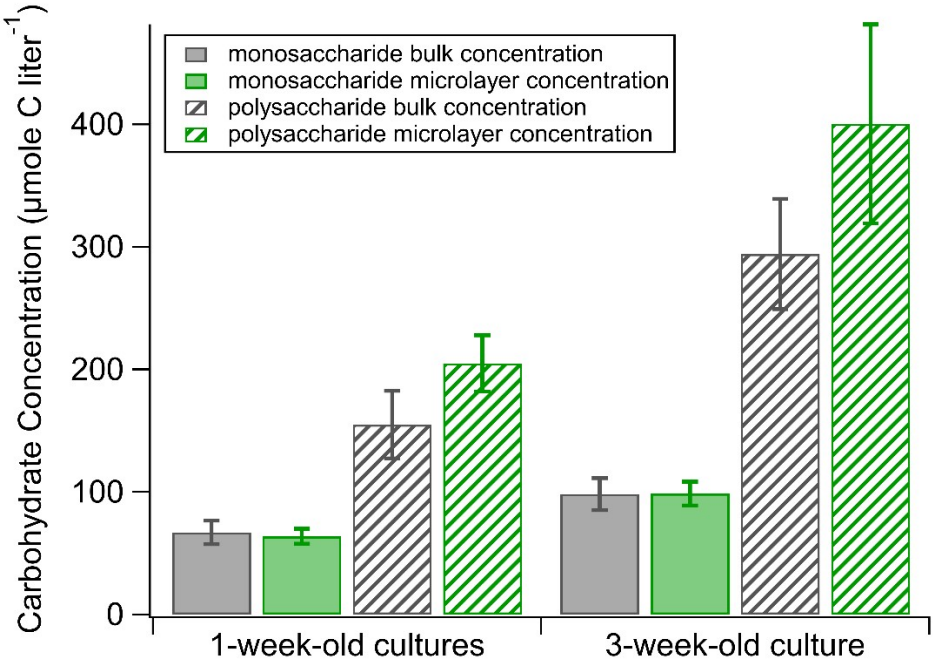

Figure S4: The measured concentration of polysaccharides and monosaccharides in 1-week old vs 3-week-old Thalassiosira pseudonana cultures in the bulk solution and the culture microlayer. The relative ratio between the bulk and the microlayer is shown in the boxes below the measurements.

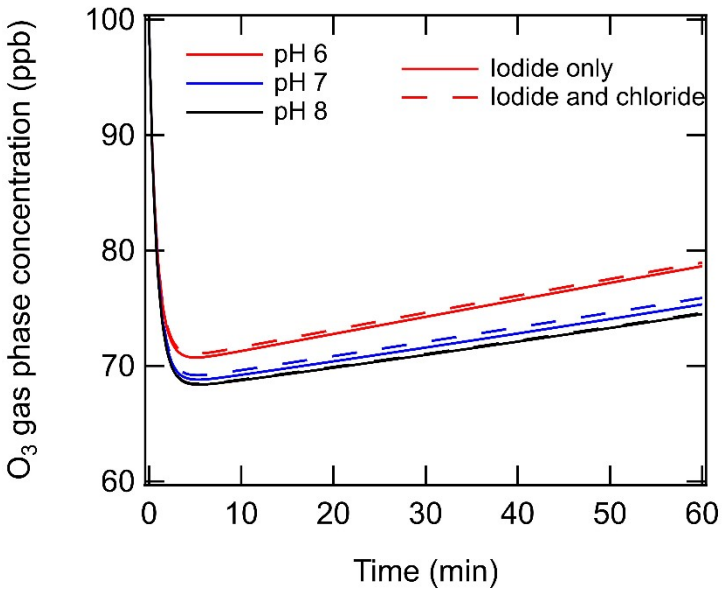

Figure S5: The estimated O_3 gas phase concentration in the flow tube outputted using the KM-SUB model when using literature rate coefficients.

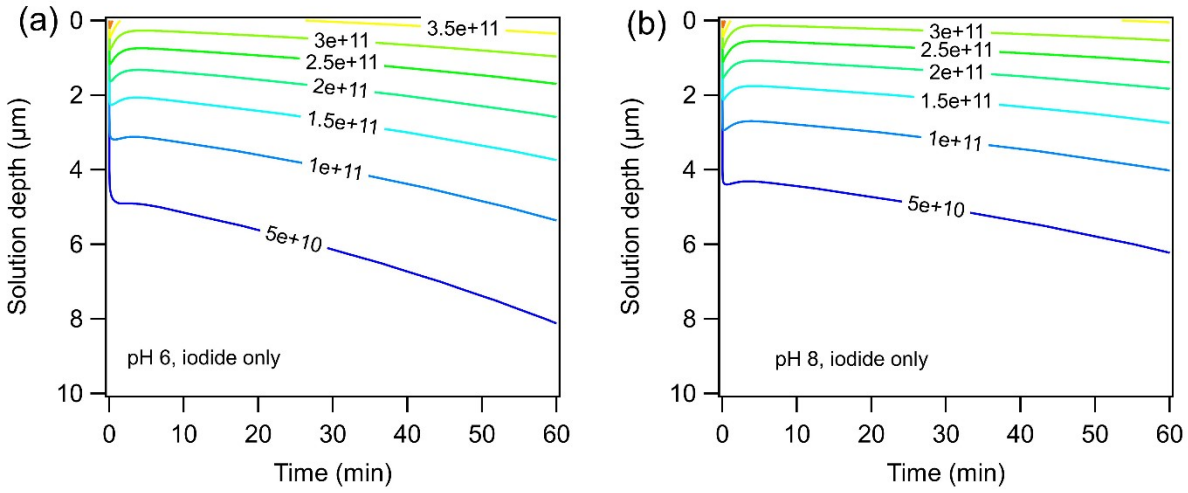

Figure S6: The bulk concentration profile of O_3 as a function of time outputted by the KM-SUB model for (a) pH 6 and (b) pH 8 for the iodide only condition and using literature rate coefficients.

VOI Measurements

	Reaction	n	k_0 [$(M^{1-n})\ s^{-1}$]	Reference
1	$HOI + Cl^- + H^+ \rightarrow ICl$	3	2.9×10^{10}	Wang et al. (1989)
2	$ICl \rightarrow HOI + Cl^- + H^+$	1	2.4×10^{6}	Wang et al. (1989)
3	$HOCl + I^- + H^+ \rightarrow ICl$	3	3.5×10^{11}	Nagy et al. (1988)
4	$I^- + O_3\ (+ H^+) \rightarrow HOI$	2	1.2×10^{9}	Liu et al. (2001)
5	$HOI + HOCl \rightarrow HIO_2 + Cl^- + H^+$	2	5.0×10^{5}	Citri and Epstein (1988)
6	$HOI + HOI \rightarrow HIO_2 + I^- + H^+$	2	2.5×10^{1}	Schmitz (2004)
7	$HIO_2 + I^- + H^+ \rightarrow HOI + HOI$	3	2.0×10^{10}	Edblom et al. (1987)
8	$HIO_2 + HOCl \rightarrow IO_3^- + Cl^- + 2H^+$	2	1.5×10^{3}	Lengyel et al. (1996)
9	$HIO_2 + HOI \rightarrow IO_3^- + I^- + 2H^+$	2	2.4×10^{2}	Furrow (1987)
10	$IO_3^- + I^- + 2H^+ \rightarrow HIO_2 + HOI$	4	1.2×10^{3}	Schmitz (2000)
11	$Cl^- + O_3\ (+ H^+) \rightarrow HOCl$	2	1.1×10^{-3}	Levanov et al. (2019)

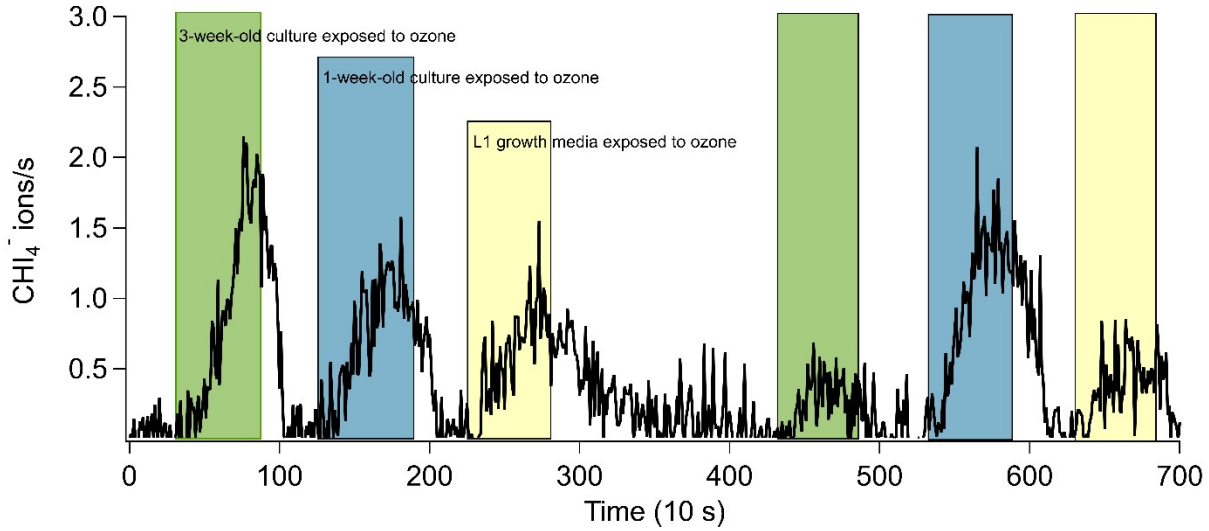

Figure S7: Measurement of CHI_4^-, which is assumed to be the iodide-iodoform adduct. There is an increase in the signal during the exposure to ozone of the 3-week-old cultures (green), 1-week-old cultures (blue) and the L1 growth media (yellow).

Reactions Included in the KM-SUB Model

12	$ICl + Cl^- \rightarrow ICl_2^-$	2	1×10^8	Margerum et al. (1986)
13	$ICl_2^- \rightarrow ICl + Cl^-$	1	6×10^5	Margerum et al. (1986)
14	$I_2 + Cl^- \rightarrow I_2Cl^-$	2	8.33×10^4	Margerum et al. (1986)
15	$I_2Cl^- \rightarrow I_2 + Cl^-$	1	5×10^4	Margerum et al. (1986)
16	$I^- + ICl \rightarrow I_2Cl^-$	2	1.1×10^9	Margerum et al. (1986)
17	$I_2Cl^- \rightarrow I^- + ICl$	1	1.5	Margerum et al. (1986)
18	$I_2 + I^- \rightarrow I_3^-$	2	6.2×10^9	Lengyel et al (1993)
19	$I_3^- \rightarrow I_2 + I^-$	1	8.9×10^6	Palmer et al. (1994)
20	$I_2 (+ H_2O) \rightarrow HOI_2^- + H^+$	1	3.2	Lengyel et al (1993)
21	$HOI_2^- + H^+ \rightarrow I_2 + H_2O$	2	2×10^{10}	Lengyel et al (1993)
22	$I_2 (+ H_2O) \rightarrow H_2OI^+ + I^-$	1	1.2×10^{-1}	Lengyel et al (1993)
23	$H_2OI^+ + I^- \rightarrow I_2 + H_2O$	2	1×10^{10}	Lengyel et al (1993)
24	$I_2 + OH^- \rightarrow HOI + I^-$	2	7×10^4	Sebök-Nagy and Körtvélyesi (2004)
25	$HOI + I^- \rightarrow I_2 + OH^-$	2	2.1×10^3	Sebök-Nagy and Körtvélyesi (2004)
26	$HOI_2^- \rightarrow HOI + I^-$	1	1.34×10^6	Lengyel et al (1993)
27	$HOI + I^- \rightarrow HOI_2^-$	2	4×10^8	Lengyel et al (1993)
28	$H_2OI^+ \rightarrow HOI + H^+$	1	9×10^8	Lengyel et al (1993)
29	$HOI + H^+ \rightarrow H_2OI^+$	2	2×10^{10}	Lengyel et al (1993)
30	$HOI \rightarrow IO^- + H^+$	1	1×10^{-1}	Paquette et al. (1986)
31	$IO^- + H^+ \rightarrow HOI$	2	1×10^{10}	Paquette et al. (1986)
32	$HOI + IO^- \rightarrow HIO_2 + I^-$	2	1.5×10^1	Bischel and von Gunten (2000)

Table S1: Reactions included in the KM-SUB model. The reactions highlighted in grey can be set to 0 and have no effect on the final concentration of $I_{2(g)}$ observed.

Estimation of I-CIMS sensitivity to $ICl_{(g)}$

The I-CIMS was previously calibrated to Cl_2. I_2 and Cl_2 have similar sensitivities on this instrument (7.6 ions/ppt and 3.7 ions/ppt, respectively), so we can assume that ICl would be comparable. From Table S3, we expect two orders of magnitude less of ICl compared to I_2 at pH 8. We don't expect to be sensitive to ICl.

Product Distribution from the KM-SUB model

Solution	pH	O_3	I^-	HOI	I_2	ICl	HOCl	HIO_2	IO_3^-	ICl_2^-	I_2Cl^-	I_3^-	HOI_2^-	H_2IO^+	IO^-
KI	6	3.06E-4	1.90E+2	7.02E+1	2.46E+1	0	0	2.75E-2	3.74E-4	0	0	3.26E-3	3.94E-3	2.94E-4	7.02E-4
	7	2.43E-4	2.26E+2	1.32E+2	5.54	0	0	3.73E-1	9.73E-3	0	0	8.72E-4	8.86E-3	2.94E-4	1.32E-2
	8	2.30E-4	2.36E+2	1.47E+2	6.53E-1	0	0	6.73E-1	1.91E-2	0	0	1.04E-4	1.03E-2	3.28E-5	1.47E-1
KI + NaCl	6	3.32E-4	1.77E+2	2.91E+1	2.26E+1	1.93E-1	3.25E-6	4.99E-3	2.59E-5	1.77E+1	2.07E+1	2.78E-3	1.54E-3	6.47E-4	2.91E.4
	7	2.62E-4	2.11E+2	1.02E+2	9.51	6.79E-2	1.93E-6	2.24E-1	4.37E-3	6.23	8.71	1.40E-3	6.41E-3	2.27E-4	1.02E-2
	8	2.32E-4	2.34E+2	1.43E+2	1.46	9.50E-3	1.32E-6	6.30E-1	1.72E-2	8.71E-1	1.34	2.38E-4	9.91E-3	3.18E.5	1.43E-1
KI + NaCl 15/100	6	3.10E-4	1.78E+2	3.26E+1	8.42E-1	2.17E-1	2.73E-6	6.19E-3	3.41E-5	1.99E+1	7.70E+1	1.04E-4	1.68E-3	7.24E-4	3.26E-4
	7	2.52E-4	2.12E+2	1.07E+2	3.34E-1	7.10E-2	1.72E-6	2.37E-1	4.69E-3	6.51	3.05E+1	4.93E-5	6.71E-3	2.38E-4	1.07E-2
	8	2.31E-4	2.33E+2	1.43E+2	4.97E-2	9.52E-3	1.20E-6	6.31E-1	1.72E-2	8.73E-1	4.54E+1	8.07E-6	9.92E-3	3.18E-5	1.43E-1
KI + NaCl 17*100	6	2.38E-4	2.29E+2	8.70E+1	2.92	5.78E-1	1.23E-6	3.64E-2	6.58E-4	5.30E+1	2.67	4.65E-4	5.83E-3	1.93E-3	8.70E-4
	7	2.30E-4	2.35E+2	1.40E+2	4.87E-1	9.34E-2	1.27E-6	4.14E-1	1.15E-2	8.56	4.46E-1	7.99E-5	9.80E-3	3.12E-4	1.40E-2
	8	2.28E-4	2.37E+2	1.51E+2	5.31E-2	1.00E-2	1.24E-6	6.94E-1	1.98E-2	9.19E-1	9.19E-1	8.77E-6	1.06E-2	3.35E-5	1.51E-1

Table S2: Aqueous concentration of all the major iodinated products after 25 minutes of model runtime. All concentrations are in units of nM.

Solution	pH	I_2	HOI	ICl
KI	6	6.440	0.322	0
	7	1.567	0.539	0
	8	0.191	0.595	0
KI + NaCl	6	6.674	0.156	0.027
	7	2.755	0.437	0.007
	8	0.439	0.580	0.001
KI + NaCl 15/100	6	0.308	0.188	0.032
	7	0.109	0.472	0.008
	8	0.016	0.585	0.001
KI + NaCl 17*100	6	0.873	0.353	0.060
	7	0.148	0.565	0.010
	8	0.016	0.604	0.001

Table S3: Gas-phase concentration of iodine from the KM-SUB model. All numbers are in ppb.

	L1 growth media concentration (M)	Concentration in final solution exposed to ozone (M)
$NaNO_3$	3.62×10^{-5}	9.05×10^{-7}
$NaH_2PO_4 \cdot H_2O$	3.62×10^{-5}	9.05×10^{-7}
$Na_2SiO_3 \cdot 9\ H_2O$	1.06×10^{-4}	2.65×10^{-6}
$Na_2EDTA \cdot 2H_2O$	1.17×10^{-5}	2.925×10^{-7}
$FeCl_3 \cdot 6H_2O$	1.17×10^{-5}	2.925×10^{-7}
$MnCl_2 \cdot 4\ H_2O$	9.00×10^{-7}	22.5×10^{-8}
$ZnSO_4 \cdot 7H_2O$	5.00×10^{-8}	12.5×10^{-9}
$CoCl_2 \cdot 6H_2O$	5.00×10^{-8}	12.5×10^{-9}
$CuSO_4 \cdot 5H_2O$	1.00×10^{-8}	2.5×10^{-10}
$Na_2MoO_4 \cdot 2H_2O$	8.22×10^{-8}	20.55×10^{-9}
H_2SeO_3	1.00×10^{-8}	2.5×10^{-10}
$NiSO_4 \cdot 6H_2O$	1.00×10^{-8}	2.5×10^{-10}
Na_3VO_4	1.00×10^{-8}	2.5×10^{-10}
K_2CrO_4	1.00×10^{-8}	2.5×10^{-10}
thiamine · HCl (vit. B1)	2.96×10^{-7}	7.4×10^{-9}
biotin (vit. H)	2.05×10^{-9}	5.125×10^{-11}
cyanocobalamin (vit. B12)	3.69×10^{-10}	9.225×10^{-12}

Table S4: L1 growth media concentrations, compared to the concentrations after dilution with the salt solution which is exposed to ozone. The recipe for the growth medium was developed by Guillard and Hargraves (1992).[8]

Parameters used in the KM-SUB model

Table S5: Parameters used in the KM-SUB model

Parameter and units	Description	Value	Source or comment
t_{res} (s)	O_3 residence time in the flow tube	83	experimentally
t_{exp} (min)	total time that the solution was exposed to O_3	60	experimentally
V (cm^3)	volume of gas in the flow tube	594.14	experimentally
S (cm^2)	surface area of the solution	227.5	experimentally
T (cm)	thickness of the solution	0.88	experimentally
$[O_3]_{g,0}$ (ppb)	O_3 concentration entering the flow tube	100	experimentally
α	surface mass accommodation of O_3, I_2, ICl and HOI	1	Vieceli et al.[19] All molecules assumed to have the same value.
τ (ns)	desorption lifetime of O_3, I_2, ICl and HOI	0.1	Vieceli et al.[9] All molecules assumed to have the same value. Also see discussion in Schneider et al.[10]
$[I^-]_{interface}$ (cm^{-2})	initial I^- interfacial concentration	1.40×10^7 (for a 390	calculated as the bulk concentration

		nM solution)	multiplied by the thickness of one iodide, chloride or H^+ ion.
$[Cl^-]_{interface}$ (cm^{-2})	initial Cl^- interfacial concentration	1.29×10^{13} (for a 0.55 M solution)	
$[H^+]_{interface}$ (cm^{-2})	initial H^+ interfacial concentration	7.13×10^6 (pH6), 7.13×10^5 (pH7), 7.13×10^4 (pH8)	
D_{O3} ($cm^2\ s^{-1}$)	O_3 bulk diffusion coefficient	1.6×10^{-5}	Johnson and Davis.[11] Note that the diffusion coefficient of I_2, Cl^-, HOCl and H^+ were also assumed to have the same diffusion coefficient.
D_{I^-} ($cm^2\ s^{-1}$)	I^- bulk diffusion coefficient	1.5×10^{-5}	Mohammad et al.[12] Note that all other molecules and ions not listed above were assumed to have this diffusion coefficient.
H_{O3} ($M\ atm^{-1}$)	O_3 Henry's law coefficient	8.6×10^{-3}	NASA JPL Handbook, with salt correction applied.[13]
H_{I2} ($M\ atm^{-1}$)	I_2 Henry's law coefficient	3.1	Sander et al.[14]
H_{ICl} ($M\ atm^{-1}$)	ICl Henry's law coefficient	111	Sander et al.[14]
H_{HOI} ($M\ atm^{-1}$)	HOI Henry's law coefficient	415	Sander et al.[14]

References

(1) Zhang, W.; Zhang, H. Secondary Ion Chemistry Mediated by Ozone and Acidic Organic Molecules in Iodide-Adduct Chemical Ionization Mass Spectrometry. *Anal. Chem.* **2021**, *93* (24), 8595–8602.

(2) Dörich, R.; Eger, P.; Lelieveld, J.; Crowley, J. N. Iodide CIMS and *m/z* 62: The Detection of HNO_3 as NO_3^- in the Presence of PAN, Peroxyacetic Acid and Ozone. *Atmos. Meas. Tech.* **2021**, *14* (8), 5319–5332.

(3) Harvey, G. W.; Burzell, L. A. A SIMPLE MICROLAYER METHOD FOR SMALL SAMPLES1. *Limnol. Oceanogr.* **1972**, *17* (1), 156–157.

(4) Myklestad, S. M.; Skånøy, E.; Hestmann, S. A Sensitive and Rapid Method for Analysis of Dissolved Mono- and Polysaccharides in Seawater. *Mar. Chem.* **1997**, *56* (3), 279–286.

(5) Schneider, S. R.; Collins, D. B.; Lim, C. Y.; Zhu, L.; Abbatt, J. P. D. Formation of Secondary Organic Aerosol from the Heterogeneous Oxidation by Ozone of a Phytoplankton Culture. *ACS Earth Space Chem.* **2019**, *3* (10), 2298–2306.

(6) Wurl, O.; Holmes, M. The Gelatinous Nature of the Sea-Surface Microlayer. *Mar. Chem.* **2008**, *110* (1), 89–97.
(7) Wong, J. P. S.; Carslaw, N.; Zhao, R.; Zhou, S.; Abbatt, J. P. D. Observations and Impacts of Bleach Washing on Indoor Chlorine Chemistry. *Indoor Air* **2017**, *27* (6), 1082–1090.
(8) Guillard, R. R. L.; Hargraves, P. E. Stichochrysis Immobilis Is a Diatom, Not a Chrysophyte. *Phycologia* **1993**, *32* (3), 234–236.
(9) Vieceli, J.; Roeselova, M.; Potter, N.; Dang, L. X.; Garrett, B. C.; Tobias, D. J. Molecular Dynamics Simulations of Atmospheric Oxidants at the Air-Water Interface: Solvation and Accommodation of OH and O3. *J. Phys. Chem. B* **2005**, *109* (33), 15876–15892.
(10) Schneider, S. R.; Lakey, P. S. J.; Shiraiwa, M.; Abbatt, J. P. D. Reactive Uptake of Ozone to Simulated Seawater: Evidence for Iodide Depletion. *J. Phys. Chem. A* **2020**, *124* (47), 9844–9853.
(11) Johnson, P. N.; Davis, R. A. Diffusivity of Ozone in Water. *J. Chem. Eng. Data* **1996**, *41* (6), 1485–1487.
(12) Mohammad, M.; Lubna Naz, L.; Tariq, M.; Qadri, M. S.; Latif, M.; Tahiri, I. A. Diffusion Coefficient of Iodide Ions in Aqueous Medium and in Vacuum: An Appraisal. *J. Chem. Soc. Pak.* **2015**, *37* (3), 440–446.
(13) Burkholder, J. B.; Sander, S. P.; Abbatt, J. P. D.; Barker, J. R.; Huie, R. E.; Kolb, C. E.; Kurylo, M. J.; Orkin, V. L.; Wilmouth, D. M.; Wine, P. H. *Chemical Kinetics and Photochemical Data for Use in Atmospheric Studies: Evaluation Number 18*; NASA, 2015.
(14) Sander, R. Compilation of Henry's Law Constants (Version 4.0) for Water as Solvent. *Atmos. Chem. Phys.* **2015**, *15* (8), 4399–4981.